Supporting Information

Scanning SAXS/WAXS microscopy selectively probes HA content in gelatin/hydroxyapatite scaffolds for osteochondral defect repair

D. Altamura[1], S. Pastore[1], M.G. Raucci[2], D. Siliqi[1], F. De Pascalis[3], M. Nacucchi[3], L. Ambrosio[2,4] & C. Giannini[1,*]

[1]*Institute of Crystallography (IC), National Research Council, Bari, Italy.*

[2]*Institute of Polymers, Composites and Biomaterials (IPCB), Naples, Italy.*

[3]*Italian National Agency for New Technologies, Energy and Sustainable Economic Development (ENEA), Brindisi, Italy.*

[4]*Department of Chemical Sciences and Materials Technology (DSCTM), National Research Council, Rome, Italy.*

cinzia.giannini@ic.cnr.it

- **Evaluation of the absorption trend as a function of scaffold thickness (diameter) for a given constant μ (attenuation coefficient).**

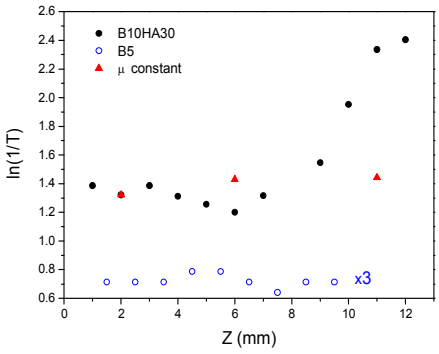

Figure S1. Plots of attenuation (ln(1/T)) registered along the z axis of B10HA30 (black dots) and B5 (blue dots) in the XMI-LAB. The red triangles represent attenuations calculated at constant μ in three points along the longitudinal axis (Z) of the B10HA30 scaffold.

The attenuation values reported in Figure S1 as triangles show the effect of scaffold diameter (measured in the three points here considered, by using a gauge) variations: the attenuation in the first point on the left was measured; then the corresponding μ value was derived based on the Lambert-Beer law, and was used in turn to calculate the attenuation in the two other points, by taking into account the relevant diameter measures. As it can be readily seen in Figure S1, at constant μ the absorption in three different points of the sample does not present significant differences (red triangles). The absorption trend observed for the B10HA30 scaffold (black points) cannot be justified by possible variations of scaffold diameter.

- **Study of porosity along the longitudinal axis of the scaffolds B10HA30 and B5**

The porosity can be computed, for each slice, from the ratio of the area of the internal pores to the total area (pores plus structure of gelatin/hydroxyapatite). Since the grayscale intensity of the region outside the sample (air) is identical to the intensity relative to the internal pores, simple thresholding is not effective to isolate the exterior from the internal pores.

In order to separate the exterior zones from the pores, the following procedure was adopted.

1) Thresholding Binarization: first the solid structure was separated from the air by using a segmentation by thresholding (Figure S2a). The appropriate value of the threshold is chosen by analyzing peaks and valleys of the tomographic data histograms in order to produce a binary image in which all the pixels inside the structure are set to one (white) and all other pixels are set to zero (black).
2) Morphological Closing: it makes a dilation (Gonzalez RC et al., 2002. *Digital Image Processing*, 2nd. Ed.) of the binarized regions, followed by an erosion. The dilation fills holes and reconnects separated regions, then the erosion restores original exterior shape. In this case a flat, disk-shaped structuring element with radius 9 (pixels) has been used in order to close the smaller holes, preserving at the same time the boundary shape of the sample (Figure S2b).
3) Remove Holes: starting from the previous image, it computes the area of all the zero-zones, then it inverts the value (from zero to ones) for all those zones whose area is under a certain threshold. Setting correctly the threshold, it is possible to separate the internal zero-zones from the exterior.

4) Arithmetic Sum: by summing the binary image in Figure S2a with the image in Figure S2c we obtain the three-values final image in Figure S2d. In such an image, the pixels belonging to the three zones (exterior air, pores and structure) assume different values and are well separated. In particular, those pixels corresponding to the solid structure assume a value equal to 2 (red), while the value associated with those pixels inside the pores internal to the sample take a value equal to one (white). The pixels belonging to the area outside the sample remain zero (black).

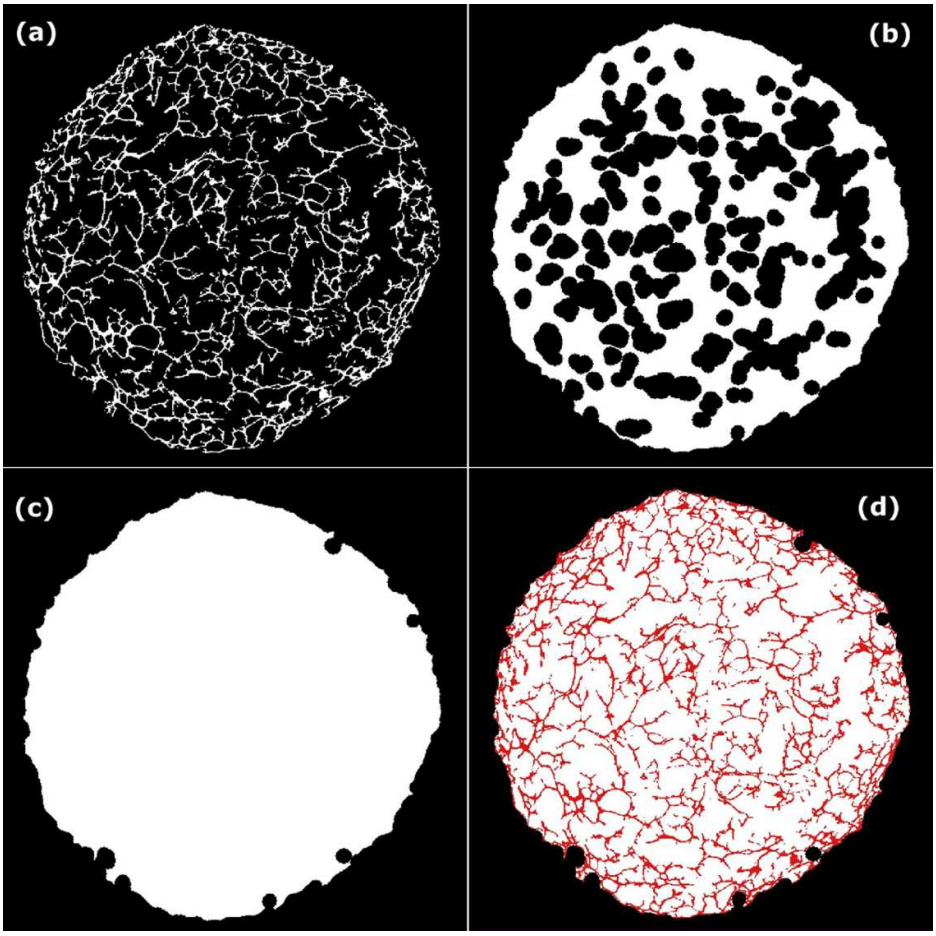

(e)

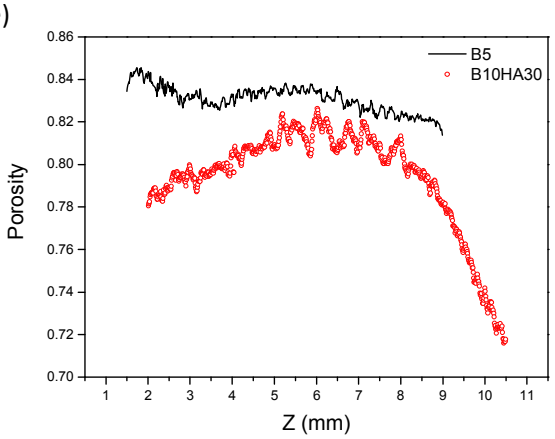

Figure S2. Flow chart for porosity evaluation on a 2D xy cross section of the B10HA30 scaffold (a-d); plots of the porosity integrated over the xy cross-sections, along the longitudinal axis of B5 (continuous line) and B10HA30 (dots) scaffolds (e).

A negative trend in porosity is found (Figure S2e), which indicates a higher density on average in the last portion of the scaffold (which will be confirmed to be associated to a higher HA concentration). On the other hand, no significant variations of the porosity is detected in the bare gelatin scaffold B5, in agreement with the absence of absorption gradients.

The slight absorption decrease in Figure 4a is mainly ascribed to a slight density decrease in the solid part of the scaffold, as it can be deduced from Figure S3, representing the mean pixel intensity of each cross-section as a function of the z coordinate: a mild decrease can be observed before z = 6 mm followed by a clear increase toward the end of the scaffold, due to the increase in HA concentration and decrease in porosity (see also Figure S2) producing the sought concentration gradient between the two ends of the scaffold.

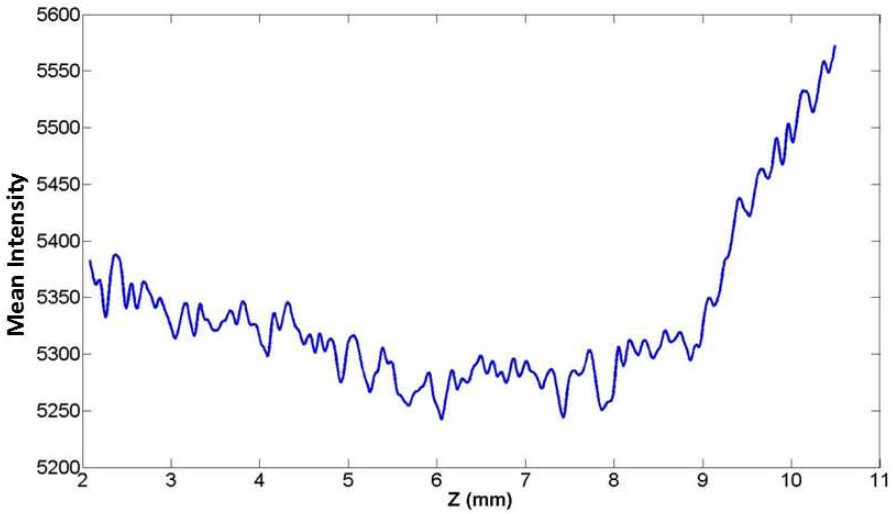

Figure S3. Plot of the area of the mean intensity per pixel, along the z axis, for the sample B10HA30.

The slight increase in porosity around z = 6 mm contributes only a small part to the mild absorption decrease in Figure 4a, as it is partially compensated by the increase in scaffold diameter. This is shown in Figure S4, where the area of the only solid part of the scaffold (without voids) has been plotted, as a function of the z coordinate, for the sample B10HA30.

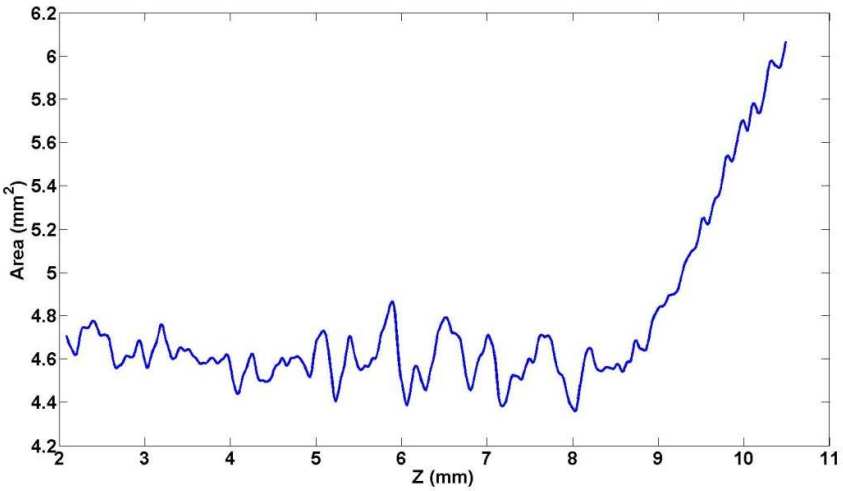

Figure S4. Plot of the area of the solid part of scaffold (without voids) along the z axis, for the sample B10HA30.

- **WAXS analysis for the B10H30 scaffold**

The size of HA nanocrystals was extimated by a Rietveld based fitting of WAXS data. An average apparent size of 9 nm was derived. The average orthogonal nanocrystal dimensions associated to the 010 and 002 diffraction peaks, i.e. the mutually orthogonal short and long directions, resulted equal to 5.5 ± 0.5 nm and 24.7 ± 0.5 nm, respectively.

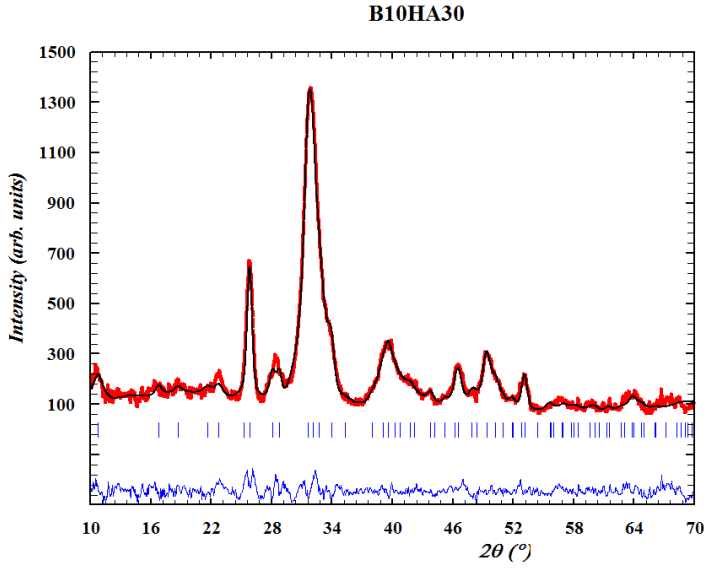

Figure S5. Example of Rietveld profile fitting obtained on a WAXS pattern from the sx2 slice of the B10HA30 scaffold.

- **Scattering maps and tissue dependent q-ranges**

In the following figures, the SAXS maps collected for each slice of B10HA30 and B5 are shown. The total scattered intensity maps, computed across the Δq_{TOT} range, and the maps recalculated by integrating the scattered intensity in the selected q ranges (Δq_{HA}: 0.03 ÷ 0.04 $Å^{-1}$, Δq_{GEL+HA}= 0.008 ÷ 0.011 $Å^{-1}$) are reported. As an example, the small highlighted areas in the maps plotted in the two q-ranges for the slice Sx2, show how the presence of HA is related to high brightness in Δq_{HA}: 0.03 ÷ 0.04 $Å^{-1}$ together with low brightness in Δq_{GEL+HA}= 0.008 ÷ 0.011 $Å^{-1}$ (red circles), whereas the presence of gel (and possibly HA) is related to high brightness regions in both q-ranges green circles) are (second row in Figure S6a). Similar indications are reported for slices of bare gelatin in Figure S6b (blue circles), showing how the scattering contribution from the bare gelatin only leads to bright regions in the Δq_{GEL+HA}= 0.008 ÷ 0.011 $Å^{-1}$ range. The notations "Sx" and "Dx" reported in the following figures indicate left and right side of the scaffold, respectively.

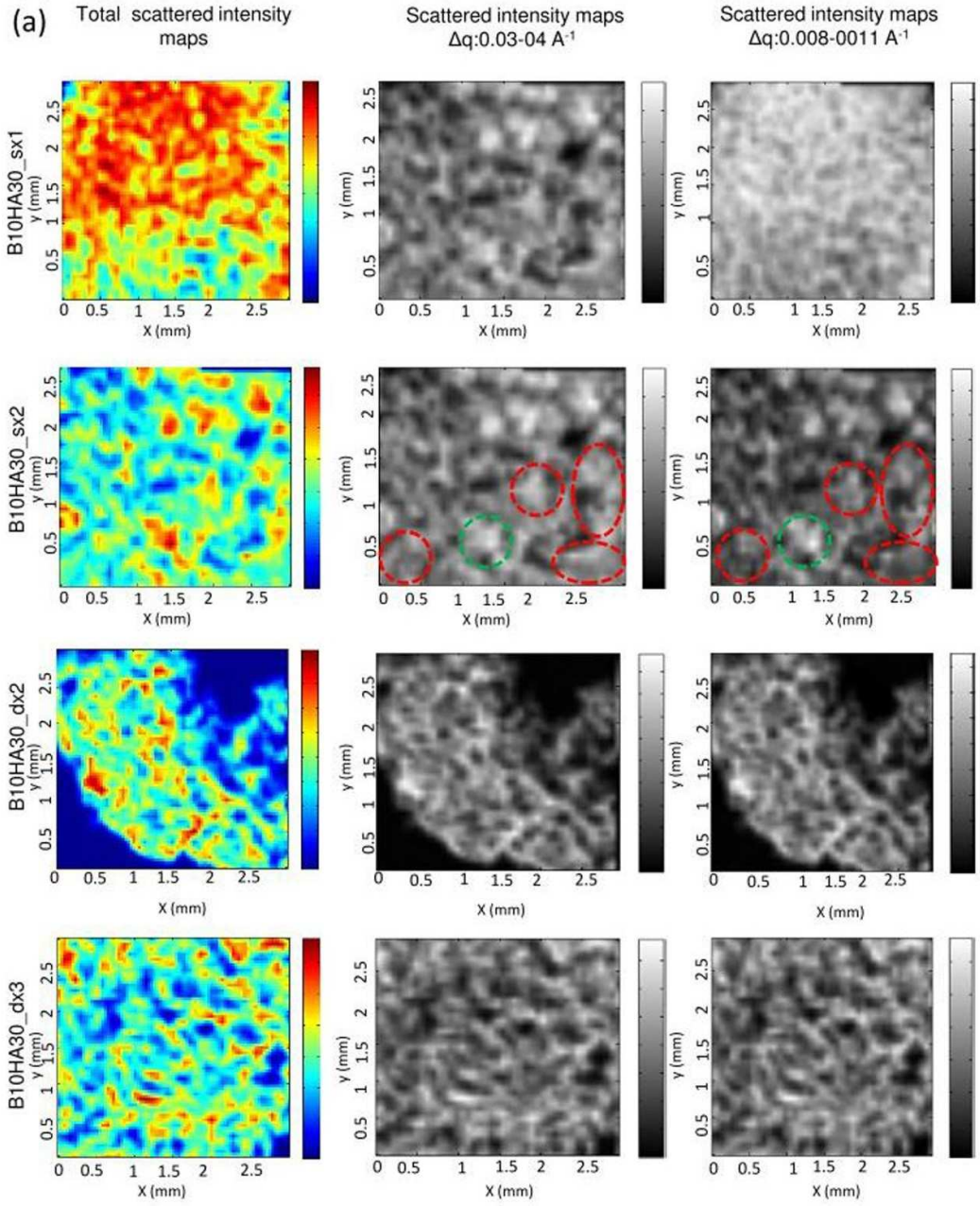

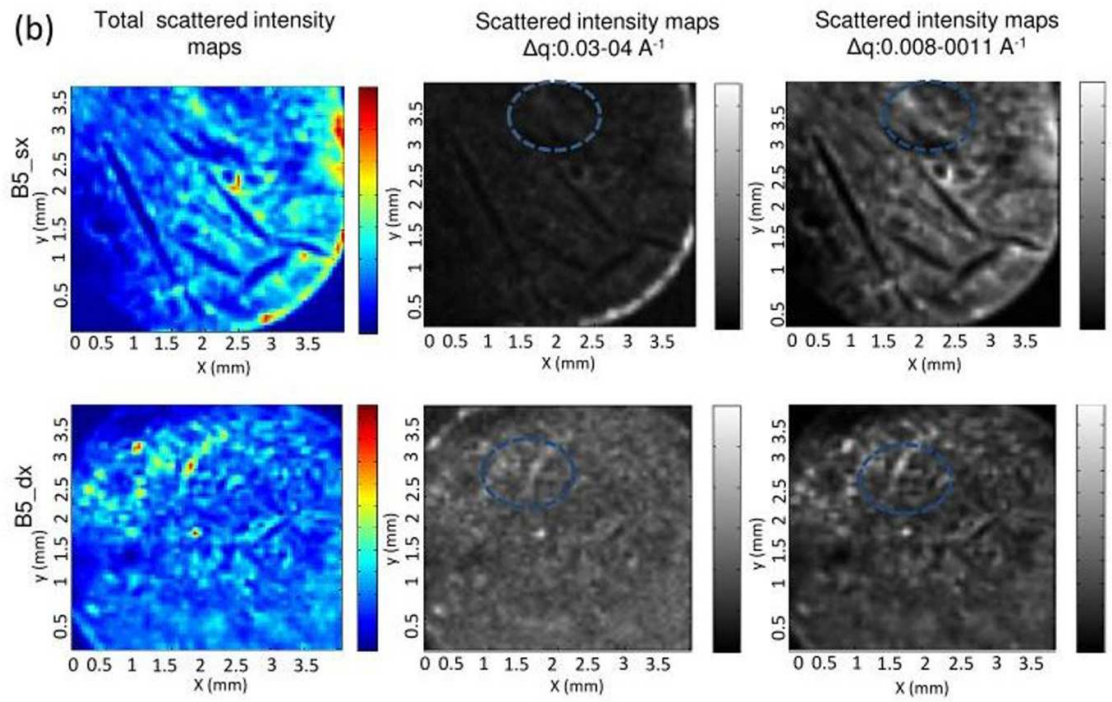

Figure S6. Total Scattered Intensity Maps, and recalculated maps in the Δq ranges 0.03 ÷ 0.04 $Å^{-1}$ and 0.008 ÷ 0.011 $Å^{-1}$, respectively, for B10HA30 (a) and B5 samples (b).

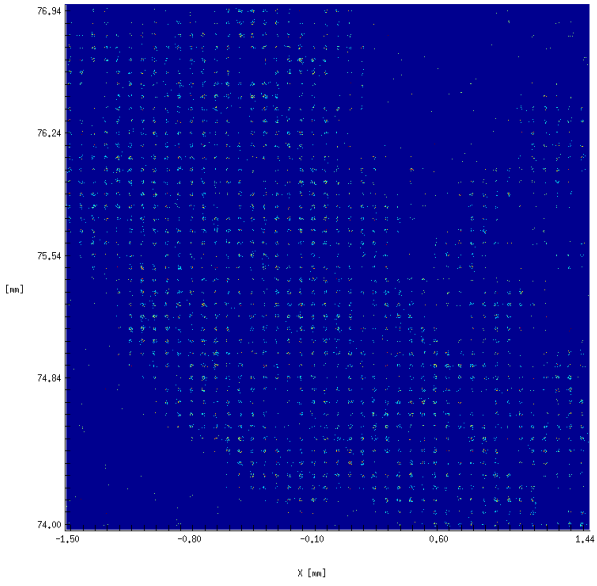

Figure S7. Composite map of a scanning SAXS measurement for the B10HA30 dx2 slice. Each pixel contains a 2D SAXS frame.

In order to compare the scattered intensity for the samples B10HA30 and B5, the following procedure has been applied:

- for each slice of the samples, 1x1 mm^2 subareas (denoted as A in the following) have been selected in the composite maps (see schemes in Figures S8, S9, where the composite maps represented in blue correspond to

the scattered intensity maps in the Figure S6) and the total scattered intensity I(A), integrated in the relevant q ranges ($\Delta q = 0.03 \div 0.04$ Å^{-1} and $\Delta q = 0.008 \div 0.011$ Å^{-1}), has been estimated all over each of the subareas, as

$$I(A) = \sum_{1}^{N_{scan}(A)} I_{scan}$$

where $N_{scan}(A)$ is the number of scans (i.e. SAXS patterns) in the generic subarea A.

- the average scattered intensity on the selected subareas along with the relative standard deviation was calculated (Tables S1, S2) for each slice, and normalized for the experimental conditions (primary beam intensity I_0, transmission coefficient T, collection time, slice thickness);

- the subareas that include empty regions or borders, leading to large deviations from the average, have been excluded from the computation; the subareas represented in Figure S8 were suitable for the evaluation of the integrated scattering intensity;

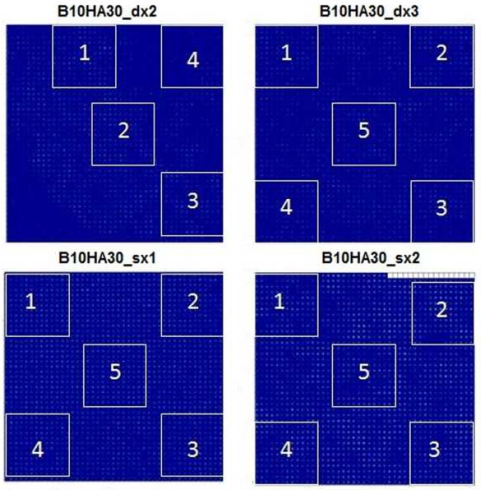

Figure S8. Composite maps of each slice for theB10HA30 scaffold, with the selected subareas (white squares) in which the scattered intensity has been integrated.

- the average scattered intensity over each slice was calculated through the summation over all of the suitable subareas A_i in that slice, and dividing by the total number of scans, as

$$< I > = \frac{\sum_1^{nA} I(A_i)}{\sum_1^{nA} N_{scan}(A_i)}$$

- the ratio between the integrated scattered intensities from the right end and left end slices was calculated for B10HA30 as

$$< I(Dx) > / < I(Sx) > = \frac{\sum_1^{nA_{Dx2}} I(A_{Dx2}) + \sum_1^{nA_{Dx3}} I(A_{Dx3})}{\sum_1^{nA_{Dx2}} N_{scan}(A_{Dx2}) + \sum_1^{nA_{Dx3}} N_{scan}(A_{Dx3})} \Big/ \frac{\sum_1^{nA_{Sx1}} I(A_{Sx1}) + \sum_1^{nA_{Sx2}} I(A_{Sx2})}{\sum_1^{nA_{Sx:}} N_{scan}(A_{Sx1}) + \sum_1^{nA_{Sx2}} N_{scan}(A_{Sx2})}$$

- the ratio between the integrated scattered intensities from the right end and left end slices was calculated, similarly to the B10HA30 sample.

Table S1. Normalized scattered intensity values computed for each subarea of each slice of B10HA30 scaffold, with the average values and the relative standard deviations. The highlighted blue values have been excluded in the computation, since they correspond to subareas with no sample.

ΔQ: 0.03-0.04	**I(B10HA30_sx1)**	**I(B10HA30_sx2)**	**I(B10HA30_dx3)**	**I(B10HA30_dx2)**
1	38,110221	29,882079	49,743911	58,61544748
2	36,269859	38,911328	52,520031	60,73276833
3	33,345677	38,107652	46,132127	52,96134528
4	32,721517	36,661342	48,453058	26,64024362
5	37,959814	33,906976	44,697401	
Average	**35,681417**	**35,493875**	**48,309306**	**57,43652037**
St. Dev.	**2,53244607**	**3,670296031**	**3,0657352**	**4,017605745**
	7%	**10%**	**6%**	**6%**
ΔQ: 0.008-0.011				
1	202,222118	250,525580	284,402792	332,644434
2	191,667718	297,561615	292,692009	335,0679408
3	171,492467	279,181418	259,443969	314,1510124
4	167,934667	277,201178	247,392741	148,0952309
5	195,628087	261,947998	260,311996	
Average	**185,789011**	**273,283558**	**268,848701**	**327,2877957**
St. Dev.	**15,203473**	**17,93026087**	**18,92165189**	**11,44113865**
	8%	**6%**	**7%**	**3%**

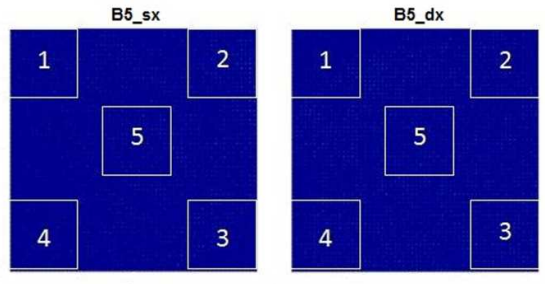

Figure S9. Composite maps of both slices of the B5 scaffold, with the selected subareas (white squares) in which the scattered intensity has been integrated.

Table S2. Normalized scattered intensity values computed in each subarea for each slice of the B5 scaffold, with the average values and the relative standard deviations. The highlighted blue values have been excluded since they correspond to subareas with no sample and have not been considered in the computation.

ΔQ: 0.03-0.04	**I(B5_sx)**	**I(B5_dx)**
1	2,769871169	2,192515
2	5,121124006	2,348857
3	5,088444282	2,845172
4	1,812095894	2,532697
5	3,588145623	2,428852
Average	**3,179008396**	**2,469619**
St. Dev.	**0,578607415**	**0,243952408**
	18%	**10%**
ΔQ: 0.008-0.011		
1	96,41895657	71,575945
2	176,8139875	101,1552
3	129,6750794	117,38673
4	51,19950006	94,704859
5	154,7645977	103,53916
Average	**125,5917771**	**97,67238**
St. Dev.	**41,25659846**	**16,77077**
	33%	**17%**

- **XRD analysis for B5 scaffold seeded with hMSCs in biomimetic conditions**

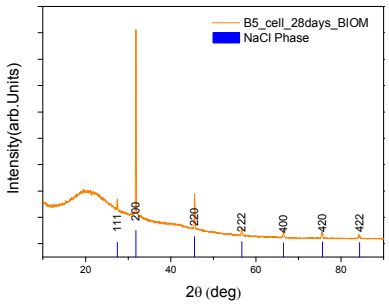

Figure S10. XRD profile of B5 scaffold treated with hMSCs for 28 days in biomimetic conditions with the relative NaCl indexing (ICSD code#018189).

In the sample treated with only hMSCs in biomimetic conditions (treatment in Simulated Body Fluid for 7 days), there is no presence of HA signal. Conversely, NaCl formation is evident from the XRD profile, due to the combination of Na^+ and Cl^- ions contained in the biomimetic solution.